AFRL-AFOSR-JP-TR-2023-0072

Study of hardening and softening characteristics in A-site acceptor- and donor-doped 0.93Bi0.5Na0.5TiO3-0.07BaTiO3 lead-free piezoceramics

SASIPOHN PRASERTPALICHAT
FACULTY OF SCIENCE NARESUAN UNIVERSITY
99 MOO 9 PHITSANULOK - NAKHON SAWAN ROAD
MUANG, , 65000
THA

03/29/2023
Final Technical Report

Air Force Research Laboratory
Air Force Office of Scientific Research
Asian Office of Aerospace Research and Development
Unit 45002, APO AP 96338-5002

REPORT DOCUMENTATION PAGE

PLEASE DO NOT RETURN YOUR FORM TO THE ABOVE ORGANIZATION.

1. REPORT DATE	2. REPORT TYPE	3. DATES COVERED	
20230329	Final	START DATE 20210924	END DATE 20221223

4. TITLE AND SUBTITLE
Study of hardening and softening characteristics in A-site acceptor- and donor-doped 0.93Bi0.5Na0.5TiO3-0.07BaTiO3 lead-free piezoceramics

5a. CONTRACT NUMBER	5b. GRANT NUMBER	5c. PROGRAM ELEMENT NUMBER
	FA2386-21-1-4130	
5d. PROJECT NUMBER	**5e. TASK NUMBER**	**5f. WORK UNIT NUMBER**

6. AUTHOR(S)
Sasipohn Prasertpalichat

7. PERFORMING ORGANIZATION NAME(S) AND ADDRESS(ES)
FACULTY OF SCIENCE NARESUAN UNIVERSITY
99 MOO 9 PHITSANULOK - NAKHON SAWAN ROAD
MUANG 65000
THA

8. PERFORMING ORGANIZATION REPORT NUMBER

9. SPONSORING/MONITORING AGENCY NAME(S) AND ADDRESS(ES)	10. SPONSOR/MONITOR'S ACRONYM(S)	11. SPONSOR/MONITOR'S REPORT NUMBER(S)
AOARD UNIT 45002 APO AP 96338-5002	AFRL/AFOSR IOA	AFRL-AFOSR-JP-TR-2023-0072

12. DISTRIBUTION/AVAILABILITY STATEMENT
A Distribution Unlimited: PB Public Release

13. SUPPLEMENTARY NOTES

14. ABSTRACT
The still unclear and inconsistent doping effects, particularly the effects of acceptor (hard) doping in BNT-based lead-free ceramics compared to PZT, are one of the reasons that have limited their usage in commercial applications. In this study, the effects of A-site Ag+ acceptor doping on the structure, dielectric, electrical conductivity and electromechanical properties of lead-free 0.93BNT-0.07BT (BNBT) ceramics (Ag100x, x=0.01?0.04) were systematically investigated. Rietveld refinement analysis revealed the coexistence of rhombohedral (R3c) and tetragonal (P4bm) phases, with an increase in P4bm phase fraction as x increased. An increasing of x value led to a significant decrease in resistivity (?1 order of magnitude) and a change from homogeneous to heterogeneous electrical microstructure. Furthermore, Ag+ doping has been found to exhibit amphoteric effects on the electromechanical properties. At low doping levels (x=0.01-0.02), the materials displayed a constricted P-E loop with a significant decrease in coercive field (Ec), and increases in dielectric loss (tan?), permittivity (?), and piezoelectric coefficient (d33), which resemble softening characteristics. In contrast, for higher doping level (x=0.03?0.04), a square P-E loop with a substantial increase Ec and a decrease in Pr, Pm was detected, along with a decrease in tan ? ,?, and d33, which are all the indication of hardening characteristics in PZT. These findings provide a better understanding of the effects of A-site acceptor doping on BNT-based ceramics, which can aid a more reliable modification of these materials for real-world applications.

15. SUBJECT TERMS

16. SECURITY CLASSIFICATION OF:			17. LIMITATION OF ABSTRACT	18. NUMBER OF PAGES
a. REPORT	b. ABSTRACT	c. THIS PAGE		
U	U	U	SAR	29

19a. NAME OF RESPONSIBLE PERSON	19b. PHONE NUMBER *(Include area code)*
TODD RUSHING	315-227-7003

Standard Form 298 (Rev.5/2020)
Prescribed by ANSI Std. Z39.18

Award Number

FA2386-21-1-4130

Report Type

Final report

Reporting Periods

24th September 2021 to 22nd March 2023

Program officer name

Dr. Todd S. Rushing

Principal Investigator name

Asst. Prof. Dr. Sasipohn Prasertpalichat

Abstract

The still unclear and inconsistent doping effects, particularly the effects of acceptor (hard) doping in BNT-based lead-free ceramics compared to PZT, are one of the reasons that have limited their usage in commercial applications. In this study, the effects of A-site Ag^+ acceptor doping on the structure, dielectric, electrical conductivity and electromechanical properties of lead-free 0.93BNT-0.07BT (BNBT) ceramics (Ag100*x*, *x*=0.01–0.04) were systematically investigated. Rietveld refinement analysis revealed the coexistence of rhombohedral (*R3c*) and tetragonal (*P4bm*) phases, with an increase in *P4bm* phase fraction as *x* increased. An increasing of *x* value led to a significant decrease in resistivity (~1 order of magnitude) and a change from homogeneous to heterogeneous electrical microstructure. Furthermore, Ag^+ doping has been found to exhibit amphoteric effects on the electromechanical properties. At low doping levels (*x*=0.01-0.02), the materials displayed a constricted *P*-*E* loop with a significant decrease in coercive field (E_c), and increases in dielectric loss (tanδ), permittivity (ε_r), and piezoelectric coefficient (d_{33}), which resemble softening characteristics. In contrast, for higher doping level (*x*=0.03−0.04), a square *P*-*E* loop with a substantial increase E_c and a decrease in P_r, P_m was detected, along with a decrease in tanδ, ε_r, and d_{33}, which are all the indication of hardening characteristics in PZT. These findings provide a better understanding of the effects of A-site acceptor doping on BNT-based ceramics, which can aid a more reliable modification of these materials for real-world applications.

Improved hardening characteristics in Ag acceptor doped $(Bi_{0.5}Na_{0.5})_{0.93}Ba_{0.07}TiO_3$ lead-free piezoelectric ceramics

Sasipohn Prasertpalichat[a,b*], Pathit Premwichit[a], Theeranun Siritanon[c], Ryan R. McQuade[d], and David P. Cann[d]

[a]*Department of Physics, Faculty of Science, Naresuan University,Phitsanulok 65000, Thailand*
[b]*Research Center for Academic Excellent in Applied Physics, Faculty of Science, Naresuan University, Phitsanulok 65000, Thailand*
[c] *School of Chemistry, Institute of Science, Suranaree University of Technology, Nakhonratchasima, Thailand 30000*
[d]*Materials Science, School of Mechanical, Industrial and Manufacturing Engineering, Oregon State University, Corvallis, Oregon 97331, USA*

**Email: sasipohnp@nu.ac.th*

The still unclear and inconsistent doping effects, particularly the effects of acceptor (hard) doping in BNT-based lead-free ceramics compared to PZT, are one of the reasons that have limited their usage in commercial applications. In this study, the effects of A-site Ag^+ acceptor doping on the structure, dielectric, electrical conductivity and electromechanical properties of lead-free 0.93BNT-0.07BT (BNBT) ceramics (Ag100*x*, *x*=0.01–0.04) were systematically investigated. Rietveld refinement analysis revealed the coexistence of rhombohedral (*R3c*) and tetragonal (*P4bm*) phases, with an increase in *P4bm* phase fraction as *x* increased. An increasing of *x* value led to a significant decrease in resistivity (~1 order of magnitude) and a change from homogeneous to heterogeneous electrical microstructure. Furthermore, Ag^+ doping has been found to exhibit amphoteric effects on the electromechanical properties. At low doping levels (*x*=0.01-0.02), the materials displayed a constricted *P-E* loop with a significant decrease in coercive field (E_c), and increases in dielectric loss (tanδ), permittivity (ε_r), and piezoelectric coefficient (d_{33}), which resemble softening characteristics. In contrast, for higher doping level (*x*=0.03−0.04), a square *P-E* loop with a substantial increase E_c and a decrease in P_r, P_m was detected, along with a decrease in tanδ, ε_r, and d_{33}, which are all the indication of hardening characteristics in PZT. These findings provide a better understanding of the effects of A-site acceptor doping on BNT-based ceramics, which can aid a more reliable modification of these materials for real-world applications.

Keywords: Lead-free BNT-BT, A-site acceptor doping, hardening characteristics, ferroelectric properties, piezoelectric properties

Introduction

"Hard-type" piezoelectric ceramic are characterized by their low dielectric loss (tan δ), high mechanical quality factor (Q_m) and high coercive field (E_c), allowing them to deliver maximum output power with low heat generation. As a consequence, "hardened" piezoceramics are highly desirable in high-power applications including sensors, ultrasonic motors, transformers and high intensity focus ultrasound (HIFU) [1] [2] [3]. From a material's perspective, lead-zirconate titanate ($Pb(Zr_{1-x}Ti_x)O_3$, PZT) and its derivatives have been the mainstay in the piezoelectric market (accounting for more than 95% of usage) due to their excellent piezoelectric properties, particularly at the morphotropic phase boundary (MPB) composition around x = 0.48 [1] [4]. In addition, the role of chemical modification through doping (both donor and acceptor) in terms of defect chemistry-property relationship, has been well established and documented, thus enabling a straightforward and reliable modification of PZT's properties for a broad range of applications [5].

Generally, hardening characteristics in PZT can be simply induced by incorporating acceptor dopants into the A-site (e.g., K^+, Na^+ replacing Pb^{2+}) or the B-site (e.g., $Mn^{2+,3+}$, $Fe^{2+,3+}$ replacing Ti^{4+}/Zr^{4+}) of the perovskite structure [6] [7] [8]. These result in a formation of negatively charged defects (e.g., Fe'_{Ti}) along with the compensating positively charged oxygen vacancies ($V_O^{\bullet\bullet}$). The mobile charged defects can exist as individual entities ($V_O^{\bullet\bullet}$, Fe'_{Ti}, e', $h^{\bullet}$) or they can couple to form defect dipole between acceptor sites and oxygen vacancies (i.e., $Fe'_{Ti} - V_O^{\bullet\bullet}$). So far, the microscopic origin of hardening effects has been ascribed to three mechanisms according to their different length scales [9] [10]. First, the "*bulk (volume)"* effect occurs from the alignment of defect dipoles along the spontaneous polarization (P_s) directions allowed by the symmetry of the phase e.g., <001> directions for tetragonal phase [11]. This results in a development of internal bias field, which subsequently leads to a stabilization of domain configuration. The second is the *domain wall effect* resulted from short-range diffusion

of charged defects to the domain wall, and the third is the *interface effect* arises from long-range diffusion of mobile charged carriers to microstructural surface boundary (e.g., grain boundaries, electrodes, pores). These two effects can also restrict the domain wall motion. Consequently, the materials exhibit hardening characteristics, which include a moderately lowered electrical resistivity (i.e., higher conductivity), a decrease in the piezoelectric coefficient (d_{33}), dielectric permittivity (ε_r) and dielectric loss (tanδ) as well as an increase in Q_m and E_c, and pronounced aging effects. [9]. Several commercial hard PZT ceramics with excellent hardening properties are available in the market such as PZT4, PZT8 [7]. However, the toxicity of lead oxide, which represents more than 70% of the weight in PZT, has raised great concern over the human health and environment, as evidenced by the directives and laws enacted to limit its usage in several countries around the globe [12] [13] [14]. Therefore, a search for lead-free piezoelectric ceramics with comparable properties to that of PZT is crucial.

Among the existing lead-free piezoelectric materials, the (1-*x*)$Bi_{0.5}Na_{0.5}TiO_3$-*x*$BaTiO_3$ [(1-*x*)BNT-*x*BT] solid solution is considered as one of the brightest candidate. This is not only due to its excellent dielectric and piezoelectric properties at the so-called MPB around *x*=0.06-0.07 compositions [15] [16] but also its simple preparation compared to another important lead-free $K_{0.5}Na_{0.5}NbO_3$ (KNN) system, which is relatively difficult to densify [17]. Effects of acceptor doping have also been extensively investigated in BNT-based materials; however, their effects don't seem to match up with conventional PZT or BT ferroelectrics. For B-site acceptor doping, even though common acceptor dopants used in PZT were adopted (e.g., Fe^{3+}, Mn^{3+}, Cu^{2+}), only moderate hardening or aging effects have been reported. For example, in a study of 1 at% Fe acceptor doped BNT-BT-KNN [18], although the $Fe'_{Ti} - V_O^{\bullet\bullet}$ defect dipole responsible for typical hard PZT were clearly detected, no significant hardening or aging was observed, which was ascribed to the pseudocubic (i.e., slightly non-cubic distortion) structure of the base composition that results in an easy switching of defect dipoles through thermal

activation. Likewise, only slight increase in E_c was observed for Fe doped BNT [19], which was also attributed to the pseudocubic nature of the host BNT. A recent study [20] investigated the effect of CuO-doped BNT-$SrTiO_3$-$BiFeO_3$. However, instead of observing the hardening properties, the dielectric and ferroelectric properties indicated a stabilization of ergodic relaxor state.

Compared to their B-site counterparts, the number of studies on A-site acceptor-doped BNT-based ceramics is limited. Most previous reports focused on the effect of A-site nonstoichiometry on electrical conductivity, due to volatility of Bi and Na during high sintering process [21] [22]. After recent finding of high values of ionic conductivity comparable to commercial ionic conductors in Bi-deficient BNT, emphasis has increasingly been paid on the improvements of BNT-based system as oxide ionic conductors through either A-site non-stoichiometry or A-site acceptor doping [23] [24]. Nevertheless, satisfying hardening properties were recently reported in a study of A-site non-stoichiometric (1-x)BNT-xBT, x=0.055, 0.06 and 0.07, ceramics. By modifying Na/Bi ratio to result in acceptor doping (i.e., Na-excess), all commonly observed "hardening" characteristics include an increase in E_c, Q_m as well as a decrease in P_r d_{33}, and tanδ were observed. Similarly, a study of A-site Li-doped BNKLT [25] have also demonstrated an increase in Q_m and E_c.

Based on these viewpoints, the morphotropic phase boundary (MPB) 0.93BNT-0.07BT, which showed the highest degree of hardening characteristics in previous A-site ratio study [26], was chosen as a starting composition. The A-site Ag^+ acceptor dopants will be incorporated to tailor defect equilibrium in the base composition, which, to the best of our knowledge, has never been investigated before. Then its effect on hardening characteristics will be investigated through systematic studies of structural, dielectric, piezoelectric, ferroelectric as well as electrical conductivity properties.

Experimental Procedure

A series of A-site Ag-doped $0.93(Bi_{0.5}Na_{0.5})TiO_3$-$0.07BaTiO_3$ ceramics based on the chemical formula $(Bi_{0.465}Na_{0.465}Ba_{0.07})_{1-x}Ag_xO_3$ where x = 0–0.04 [abbreviated as Ag100x, hereafter] were prepared via conventional solid-state reaction route. Starting raw materials were reagent-grade oxide and carbonate powders of Bi_2O_3 (99.9%, Sigma Aldrich), Na_2CO_3 (99.95%, Alfa Aesar), Ag_2CO_3 (99.5%, Alfa Aesar), TiO_2 (99%, Sigma Aldrich), $BaCO_3$ (99.9%, Alfa Aesar). The raw powders were weighted according to stoichiometric formula and ball milled with yttria-stabilized zirconia media in 99.9% ethanol for 24 h. Then, the slurries were heated in oven until dry. After that, the powder mixtures were calcined at 800 °C for 2 h, and then re-milled and dried again. The obtained calcined powders were mixed with 3 wt% polyvinyl butyral (PVB) at 1:1 ratio and uniaxially pressed into 15 mm-diameter disk-shaped pellets. The green pellets were subsequently sintered at 1150 °C in a covered alumina crucible under the air atmosphere for 2 h with the polymer burn-out step at 400 °C for 3 h. It is worth noting that the pellets were embedded in corresponding powders of each composition to suppress the loss of volatile Bi and Na elements.

The phase purity and crystal structure of all samples were examined by using laboratory X-ray diffraction (XRD, Bruker D8) with Bragg-Brentano geometry and Cu Kα radiation on the crushed sintered pellets. To obtain a higher quality data for structural refinement, the crushed sintered ceramics of each composition was further examined by synchrotron X-ray diffraction (SXRD) at beamline 1.1, synchrotron light research institute (SLRI), Thailand, with a photon energy of 12 keV (λ=1.0328 Å). The structural refinements were performed on the SXRD data by Rietveld refinement technique using Topas software. Scanning electron microscope (SEM, Leo1455VP) was utilized to study the microstructure of mirror-like polished sample surfaces thermally etched at ~100 °C below sintering temperature (i.e., 1050

°C) for 20 minutes. Prior to the characterizations of electrical properties, the sintered pellets were polished to ~0.7–0.8 mm thick and then silver paste (Heraeus C1000) were applied on both sides and fired in air at 700 °C for 30 min to form electrodes. Temperature-dependent dielectric properties were measured by LCR meter (HP, 4284A) at the frequencies of 1, 10 and 100 kHz from room temperature up to 450 °C. The AC impedance spectroscopy (IS) data were collected by impedance gain/phase analyzer (Solartron 1260) from 400 °C to 550 °C at an increment of 25 °C over the frequency range of 10 Hz 10 MHz. The bipolar polarization-electric field (*P*-*E*) hysteresis loops were measured in silicone oil at room temperature by using ferroelectric testing system (Precision Premier II, Radiant technology).

Results and Discussion

Figure 1(a) illustrates room temperature XRD patterns of Ag100*x* (*x* = 0–0.04) crushed sintered pellets at 2θ =20°–80°. Within the detection limit of the laboratory XRD used, all compositions exhibited a single-phase perovskite structure without any noticeable secondary phases. For a detailed examination, the (111) peak in the 2θ range of 39.5−40.5° and the (200) peak in the 2θ range of 46−47° were enlarged as shown in Fig 1(b) and (c), respectively. For *x*=0 (i.e., BNBT), both (111) at ~2θ=40° (Fig. 1(b)) and (200) reflections at ~2θ=46.5° (Fig. 1(c)) exhibited a single peak without any noticeable splitting or shoulder feature, implying that the sample possessed pseudocubic structure, which is in line with previous studies where 'nearly cubic' [27] or 'pseudocubic' [28] [29] were reported for the (1-*x*)BNT-*x*BT with *x*=0.06−0.07 (i.e., the MPB composition). With increasing Ag^+ doping concentration from *x*=0.01 to 0.04, the profile shape of both (111) and (200) peaks remained almost the same, suggesting that pseudocubic structure persisted for the whole range of doping level studied. It is noteworthy that the long-range structure which appear to be 'pseudocubic' in BNT-based ceramics is essentially composed a very small noncubic distortion, whose dimension is below

the detection limit of the XRD technique. The identity of this noncubicity at the local scale was revealed by multiple techniques to consist of polar nanoregions (or polar nanodomains) with the coexistence of rhombohedral (*R3c*) and tetragonal (*P4bm*) symmetries [30] [31]. In addition to this, a close inspection of the (111) and (200) peaks exhibited a shift toward higher 2θ angle with increasing *x*, thus suggesting the lattice shrinkage. This can be attributed to the smaller ionic radii of Ag^{+} (1.28 Å) which substitutes larger Ba^{2+} (1.61 Å) Bi^{3+} (1.38 Å) and Na^{+} (1.39 Å) ions on the A-site (12 cordinate) [32] [33]. The systematic peak shift observed, along with the absence of peaks corresponding to secondary phases, indicate that Ag^{+} has successfully incorporated into the BNBT lattice site and formed a complete solid solution.

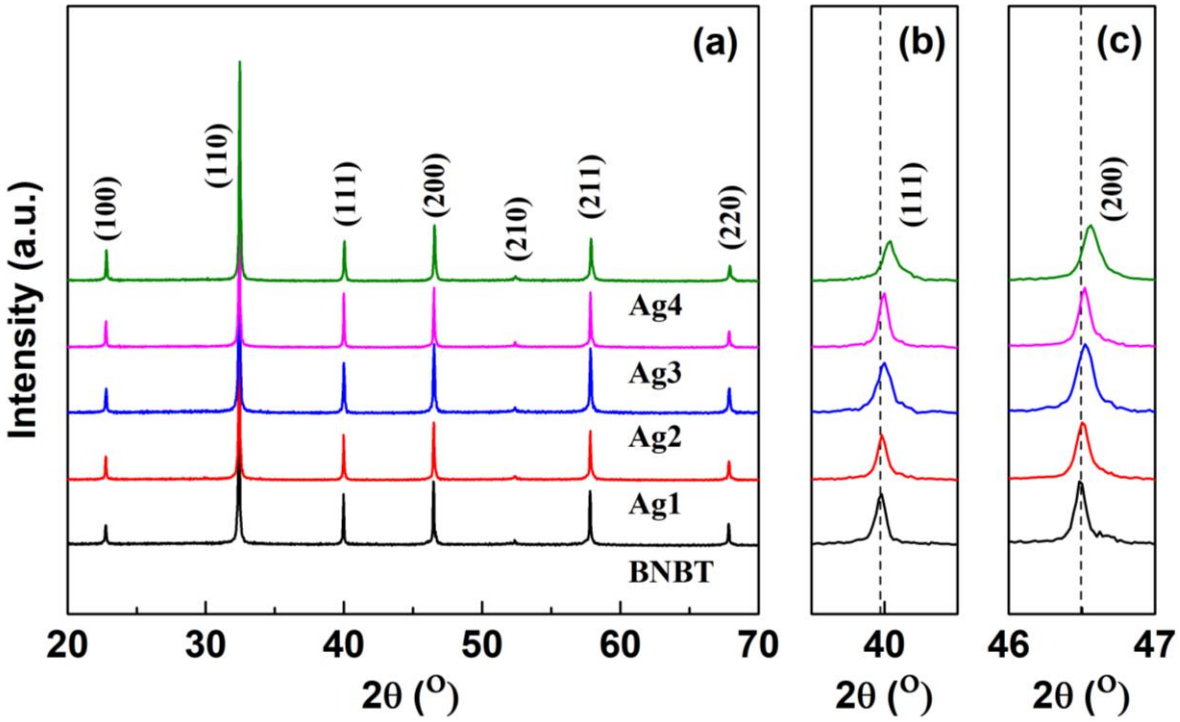

Fig. 1 Room temperature X-ray diffraction patterns of Ag100*x* and Mn100*x* (*x* = 0–0.04) crushed sintered pellets in the 2θ range of (a) 20°–80° (b) 39.5°–40.5° and (c) 46°–47°

To obtain a higher quality data for structural refinements, all samples were further examined by using synchrotron X-ray diffraction (SXRD). The SXRD patterns of Ag100*x*, *x*=0.01−0.04, compositions are shown in Figure 2(a) with the expanded view of 2θ

corresponding to (111) and (200) peaks displayed in Fig 2(b) and (c), respectively. Consistent with the abovementioned laboratory XRD data, all main features: (1) absence of impurity peaks (see Fig. 2(a)), (2) the non-existence of (111) and (200) peak splitting and (3) the upward peak shift toward higher 2Θ angle (see Fig. 2(b), (c)), were also observed from the SXRD data, thus confirming that all studied compositions crystallized into pure perovskite phase with pseudocubic structure.

To clarify the effects of Ag doping on changes in structure, full-pattern Rietveld refinement was performed on the SXRD data for all samples by using a Topas software. Due to the complex crystal structure at the MPB of BNT-BT, various two-phase models (e.g., *Cc*+*P4bm* [34], *P4mm*+*Pm*$\bar{3}$*m* [35] [36], *Cc*+*R3c* [37]) have been proposed in previous literature. Nonetheless, the combination of rhombohedral (space group *R3c*) and tetragonal (space group *P4bm*) phases provided the optimum fit in this study, which is consistent with the reported results in previous research of other BNT-BT based ceramics [38] [39] [40]. Since diffractions of *R3c* and *P4bm* phase are similar, we ensured that peak shape and broadening as a result of the phase change is correctly refined by fixing atomic coordinates and the elemental occupancies to the starting models from [41] [38] and the nominal chemical composition of the samples, respectively. The background was modeled with a Chebyshev function using eight polynomial coefficient terms. The weight percent of phase, scale factor, and lattice parameters were refined.

Resultant Rietveld refinement patterns (calculated data) of representative compositions BNBT, Ag2 and Ag4 are displayed in Fig. 3(a)−(e), respectively. The refinement results contain the *R3c* and *P4bm* phase fraction (%), the calculated lattice parameters, and the quality of refinement parameters (%$R_{wp,}$ %R_p and χ^2), as listed in Table 1. The low values of all reliability factors [goodness of fit (χ^2) = 1.45−2.11, weighted profile R-factor (R_{wp})=7.03−11.42%] indicated a high credibility of the refinement, and also confirmed that the

proposed model can well describe the experimental data. For BNBT (i.e., *x*=0) composition, the refined phase fraction (*R3c*=74.4% and *P4bm*=25.6%) agreed well with the previously reported values obtained from the Rietveld refinement analysis of either high-resolution [38] or laboratory XRD data [26]. With increasing *x*, the gradual increase in the *P4bm* phase fraction was observed. This can be seen from the data presented in Table I, which exhibits a significant increase in the *P4bm* phase fraction for Ag2 to 51.7%, a value approximately twice as high as that of the undoped composition (i.e., 25.6%). Subsequently, when *x* increased to 0.04 (Ag4), the *P4bm* phase fraction reached the maximum value of 69.3%. It is widely accepted that the *R3c* is "polar phase" [42] while the *P4bm* is "weakly polar phase" (or non-polar phase)" [43] [44]. The observed results suggest that Ag doping had a significant effect on the phase constituents of BNT-BT, causing a transition from dominant *R3c* polar phase to the dominant *P4bm* weakly polar phase. Similar result was also observed in a previous study of Li doped $0.95[0.94(BN_{(0.5-x)}Li_x)T-0.06BT]-0.05CaTiO_3$ ceramics where a considerable increase in *P4bm* phase ratio from 7% [i.e., *P4bm:R3c*=7%:93%) to 57% (i.e., *P4bm:R3c* =57%:43%) was observed when *x* increased from 0 to 0.15 [39]. Likewise, an addition of ABO_3 perovskite in (1-*x*)(BNT-BT)-*x*$NaTiO_3$ also exhibited an increase in the *P4bm* phase fraction from 50.5% (i.e., *P4bm:R3c*=50.5%:49.5%), for *x*=0, to 79.4% (i.e., *P4bm:R3c*=79.4%:20.6%), for *x*=0.15 [45].

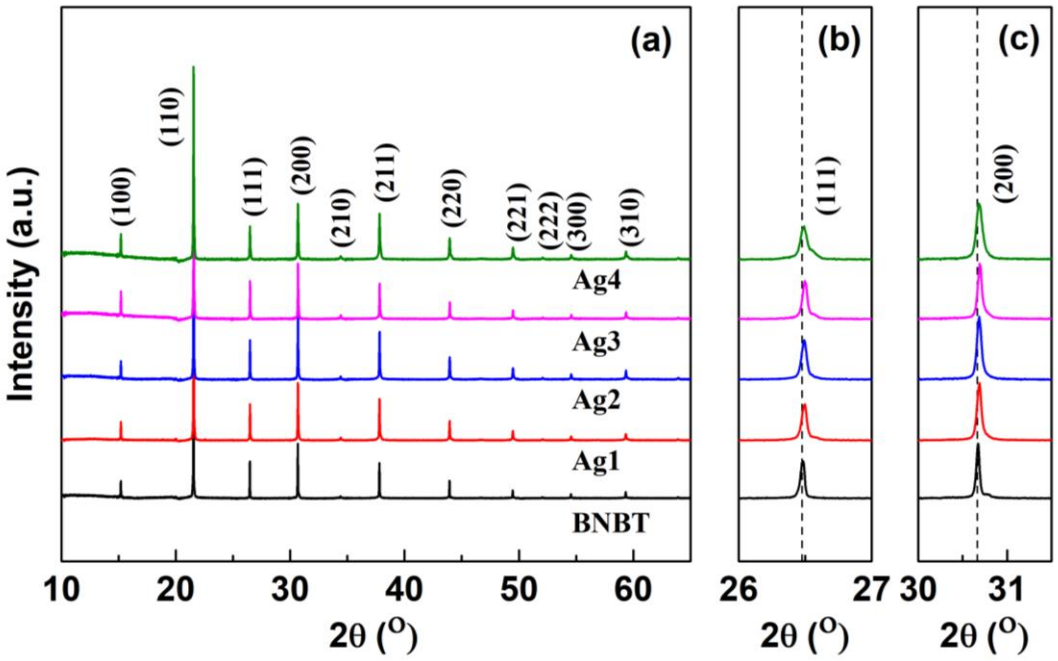

Fig. 2 Synchrotron X-ray diffraction patterns of Ag100*x* (*x* = 0–0.04) crushed sintered pellets in the 2θ range of (a) 10°–65° (b) 26°–27° and (c) 30°–31.5° measured at room temperature

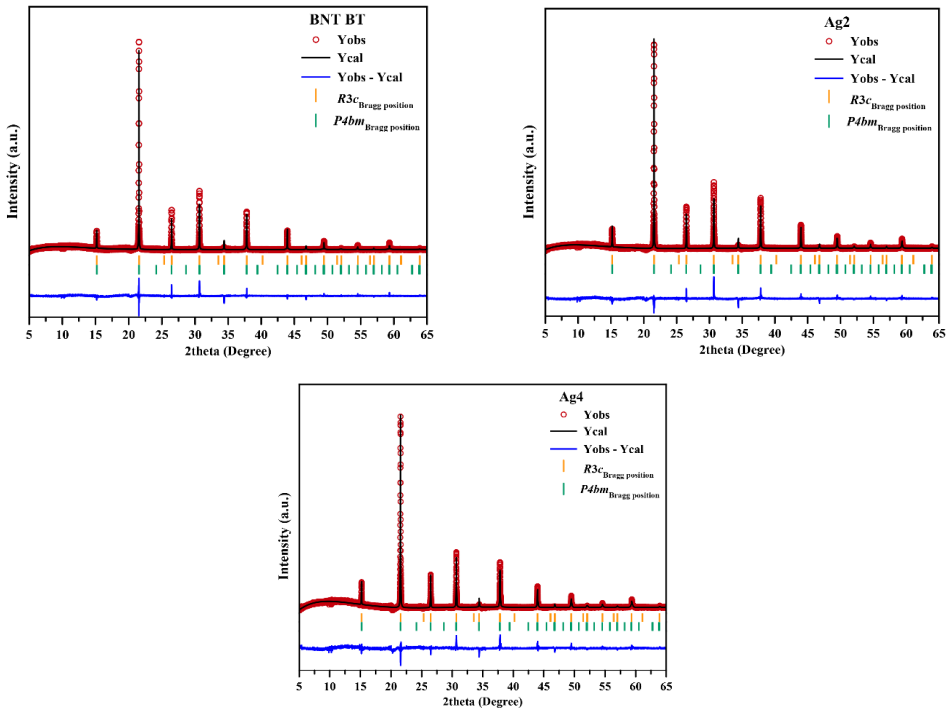

Fig. 3 Rietveld refinement patterns of Ag100*x* (*x*=0, 0.02 and 0.04) ceramics. The black circles represent the observed data, and the red lines are the calculated profile from refinement. The blue line is the difference between the observed and calculated diffraction patterns. The orange and green bars denote the allowed Bragged reflections for the space group *R3c* and *P4bm*, respectively.

Table 1. The rhombohedral (*R3c*) and tetragonal (*P4bm*) phase fraction (%), calculated lattice parameters, and the refinement quality parameters (%R_{wp}, %R_p and χ^2) obtained from Rietveld refinement of the synchrotron XRD data of BNBT-*x*Ag, *x*=0.01−0.04 samples.

	Phase fraction (%)		*R3c*			*P4bm*			%R_{wp}	%R_p	GOF
	R3c	*P4bm*	a (Å)	c (Å)	vol (Å^3)	a (Å)	c (Å)	vol (Å^3)			
BNBT	74.4	25.6	5.5199(1)	13.5201(3)	356.8	5.5203(9)	3.9099(2)	119.1	8.51	5.85	1.45
Ag1	60.9	39.1	5.5203(1)	13.5174(4)	356.7	5.5182(6)	3.9038(1)	118.9	10.96	7.35	2.11
Ag2	48.3	51.7	5.5179(1)	13.5119(6)	356.3	5.5169(4)	3.9021(6)	118.8	8.99	6.19	1.74
Ag3	68.3	31.7	5.5181(1)	13.5144(4)	356.4	5.5143(6)	3.9046(1)	118.7	7.03	4.57	1.48
Ag4	30.7	69.3	5.5173(2)	13.5131(1)	356.2	5.5169(2)	3.8967(3)	118.6	8.81	6.17	1.72

The SEM micrographs of polished and thermal-etched samples' surface of BNBT-*x*Ag, *x*=0−0.04, ceramics are illustrated in Fig. 4(a)−(e) with the insets showing grain-size distributions determined by the linear intercept method. All samples possessed dense and compact microstructure with clear grain boundaries. The combination of large and small polygon-shaped grains was also observed, which are in line with previous literature on BNT-based systems [45] [46]. The average grain size initially increased from 0.91± 0.07 µm (BNBT) to 1.17 ± 0.126 µm (Ag1) and then changed to 1.05±0.089, 0.68±0.053 and 0.75±0.064 µm for Ag2, Ag3 and Ag4, respectively. These results indicate that the addition of Ag has a minimal impact on both the average grain size and grain size distribution.

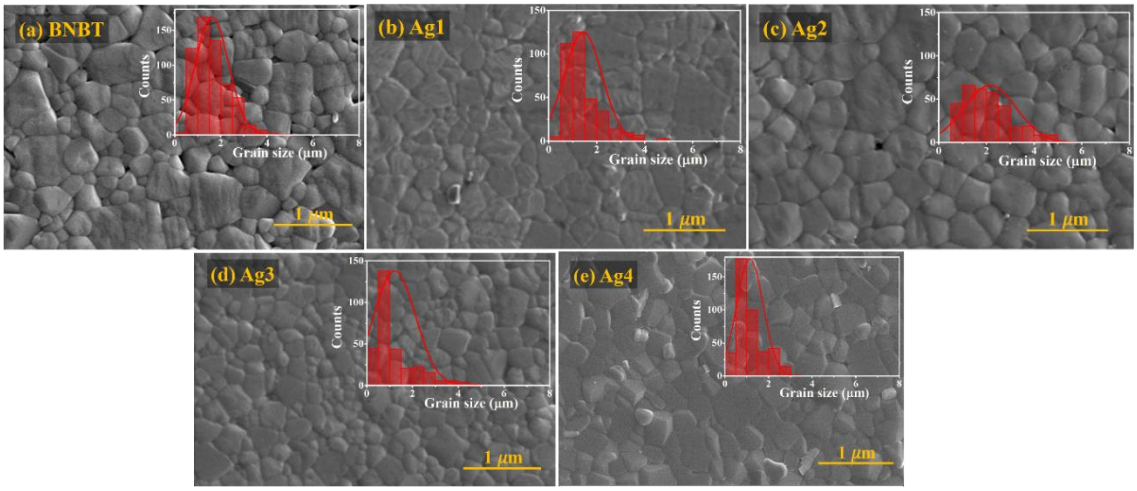

Fig. 4 SEM micrographs of Ag100*x* ceramics for (a) *x*=0, (b) *x*=0.01, (c) *x*=0.02 and (d) *x*=0.03 (e) *x*=0.04, with the inset representing the average grain size distribution for each composition.

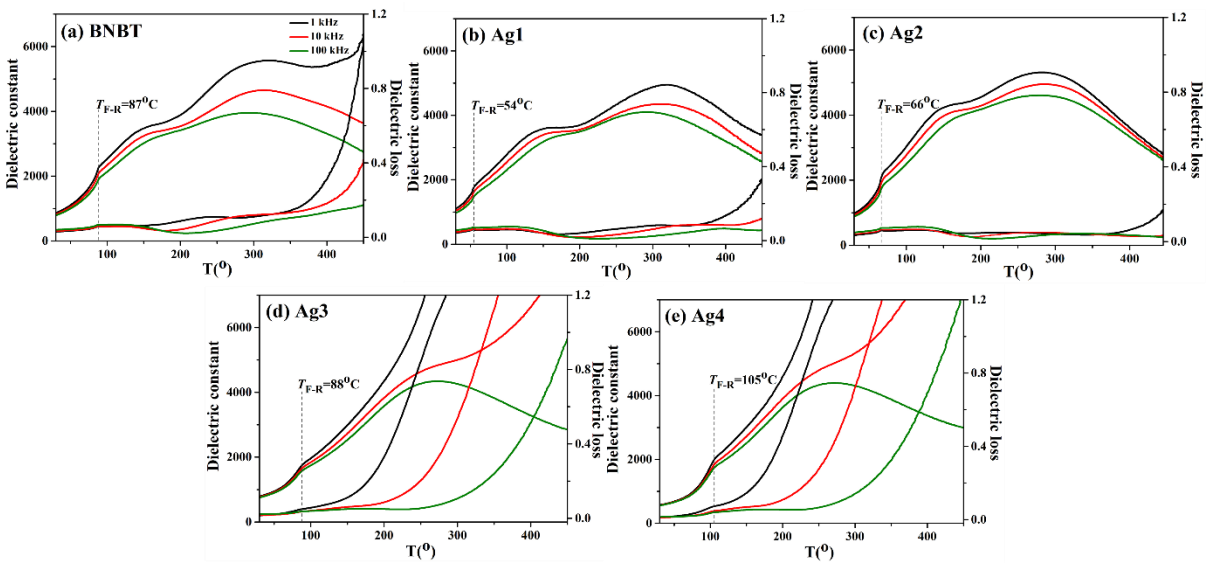

Fig. 5 Temperature dependence of dielectric permittivity (ε_r) and dielectric loss (tanδ) for poled Ag100x ceramics with (a) x=0, (b) x=0.01, (c) x=0.02 and (d) x=0.03 and (e) x=0.04

Figure 5 demonstrates the temperature dependence of relative permittivity (ε_r) and dielectric loss (tanδ) for poled Ag100x, x=0−0.04, ceramics measured at 1, 10 and 100 kHz from room temperature (RT) to 450°C. From the entire temperature and frequency range studied, two dielectric anomalies were observed. The first one at lower temperature is characterized by the frequency-independent peak in both ε_r-T and tanδ-T curves, which is referred to as the ferroelectric-to-relaxor transition temperature (T_{F-R}). The T_{F-R} is only detected in poled samples and is attributed to the converting of electric field-induced ferroelectric to its original ergodic relaxor state (ER), as evidenced by the reemergence again of frequency dispersion in ε_r-T and tanδ-T curves above the T_{F-R} [44] [47]. The second one observed at higher temperature is denoted as T_m (maximum dielectric temperature) and is identified by the frequency insensitive maximum dielectric broad peak. The origin of T_m has been recently agreed to arise from the thermal evolution of the coexistence of polar nanoregions (PNRs) with *R3c* and *P4bm* symmetries that can transform between each other with increasing temperature [44].

Extracted dielectric-property parameters including $T_{F\text{-}R}$, T_m, room temperature permittivity ($\varepsilon_{r,RT}$), maximum dielectric permittivity ($\varepsilon_{r,m}$) and their corresponding tanδ values ($\tan\delta_{RT}$ and $\tan\delta_m$) are summarized in Table 2. It is worth mentioning that the primary emphasis in this study is on the change in $T_{F\text{-}R}$ and $\tan\delta_{RT}$, which are the parameters that can be correlated with hardening properties. From Table 2 and Fig.5, the $T_{F\text{-}R}$ (marked with dotted line) initially decreased from 87°C (for BNBT) to 54°C (for Ag1) and then it monotonously increased to 66°C, 88°C and 105°C for Ag2, Ag4 and Ag4, respectively. The $T_{F\text{-}R}$ is the temperature at which electric field-induced ferroelectric order converting to ergodic relaxor state (ER) during the heat treatment [44]. Therefore, shifting of $T_{F\text{-}R}$ to higher temperature means that the disruption of FE domain to relaxor state becomes increasingly difficult (i.e., domain pattern gets more stabilized) [48] [49]. For ferroelectric perovskite oxide materials, oxygen vacancies have been generally accepted to stabilize the domain configuration [9] [10]. Thus, the observed upward shift in $T_{F\text{-}R}$ is most likely associated with an increase in oxygen vacancies resulting from increasing Ag^+ acceptor doping concentration, which will be confirmed through the following experiment in the next section. An increase in $T_{F\text{-}R}$ has also been reported in previous studies of either A-site [26] or B-site [48] acceptor-doped BNT-based materials.

Furthermore, it is well known that oxygen vacancies have a significant influence on the dielectric properties at high temperature, resulting in remarkably high values of ε_r and $\tan\delta$ [50] [51]. For Ag3 and Ag4 compositions, anomalously high ε_r and $\tan\delta$ were clearly observed at temperatures above $T_{F\text{-}R}$, and they became more apparent with increasing temperature, thus supporting the assumption of the existence of oxygen vacancies in the samples. Another supportive evidence for an increase in defect concentration in the materials from A-site acceptor doping can be seen through the change in $\tan\delta_{RT}$. Generally, the dielectric response obtained at 1 kHz regime are dominated by domain wall movement [5]. Thus, stabilized

domain will provide less contribution to the electrical response, leading to a decrease in tanδ [1] [9]. In this study, a reduction in tanδ_{RT} from 0.029 (BNBT) to 0.012 (Ag4) was clearly observed.

Table 2 Dielectric property parameters of Ag100*x*, *x*=0−0.04, ceramics determined at frequency of 1 kHz

Compositions	$T_{F\text{-}R}$ (ºC)	T_m (ºC)	$\varepsilon_{r,RT}$	tanδ_{RT}	ε_m	tanδ_m
BNBT	87	315	866	0.029	5,569	0.118
Ag1	54	320	1,113	0.041	4,948	0.082
Ag2	66	279	987	0.034	5,313	0.044
Ag3	88	255	792	0.015	6,958	0.903
Ag4	105	241	574	0.012	7,000	0.930

To examine the influence of Ag doping on the electrical conductivity and conduction mechanism, impedance spectroscopy (IS) measurements were performed on selected compositions of Ag100*x* (*x*=0, 0.02 and 0.04) at different temperatures and frequencies. Figure 6(a)−(f) display the IS data in the impedance complex plane (Z*) (i.e., Z' versus Z'') and the corresponding $Z''(f)$ spectroscopic plots (i.e., the imaginary part of the impedance (z″) versus log *f*) for BNBT, Ag2 and Ag4 measured at 425−550ºC over the frequency range of 1Hz−1MHz. The unmodified BNBT composition exhibited a single semicircle with no trace of second semicircular arc in all temperature range studied (425−550 ºC), indicating that the sample is primarily dominated by a single relaxation time relating to the grain (bulk) response. However, a slight asymmetry of arc at low frequency was also observed, suggesting a minor contribution from the grain boundary component [52]. As *x* increased to 0.02, a single semicircle with a small asymmetric semicircular arc (at low frequency) persisted. Nevertheless, a low level of depression in semicircle with its center lying below the Z′-axis started to be observed, which suggests the non-Debye-type relaxation process with distribution of relaxation times within the material [53]. When *x* reached 0.04 (Ag4), the semicircle was significantly

suppressed, showing a more prominent, asymmetric low-frequency semicircular arc. This arc continuously distorted with increasing measurement temperature and eventually developed into a small second semicircle at T≥500°C, as shown more clearly in the inset of Fig. 6(c). Beside this, the visual inspection of the semicircle's radii also demonstrates that the sample's resistance significantly decreased (~1 order of magnitude) for Ag2 and progressively decreased with further increase of *x* to 0.04 (Ag4). The observed results indicate that an introduction of Ag into the BNBT sample can significantly reduce sample's resistance and can also induce an electrically heterogenous microstructure. Furthermore, when consider the change in *Z** plot with temperature, all samples exhibited a decrease in resistance with increasing temperature as evidently observed from a decrease in Z′ values in the *Z** plots (Fig. 6(a)−(c)) and a reduction in *Z*′′ magnitudes with a shift of *Z*′′ peak toward higher frequency in the *Z*′′(*f*) plots (Fig. 6(d)−(f)). The obtained results were in line with the negative temperature coefficient of resistant (NTCR) behavior, which is the thermal activation of charge carrier process [54] usually observed in semiconductors and BNT-based systems [55] [56].

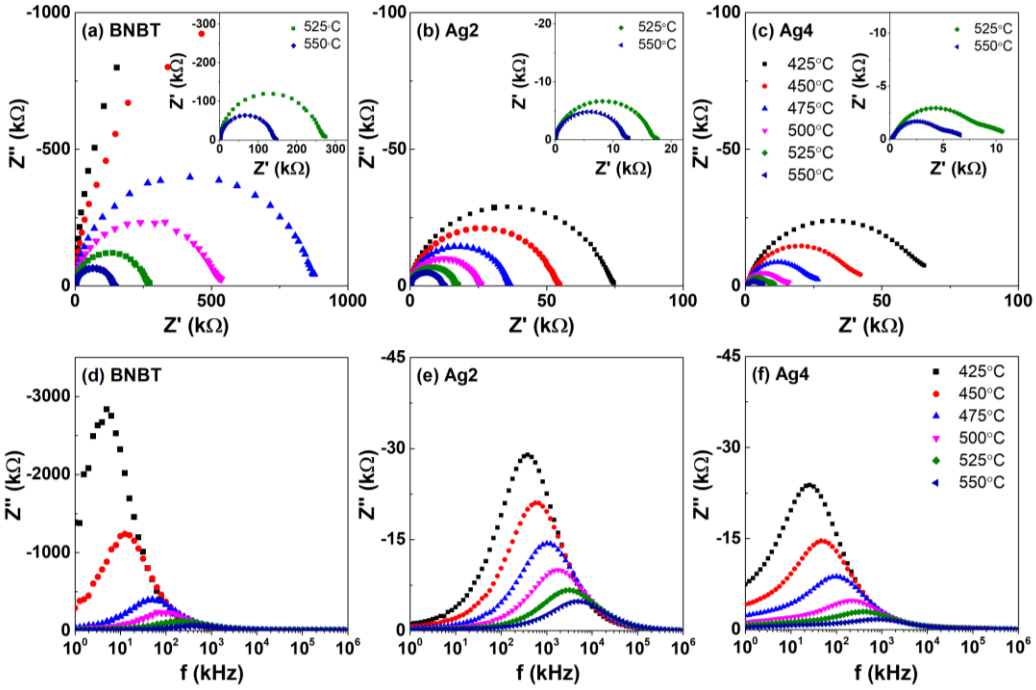

Fig. 6 Impedance complex plane (*Z**) plots and corresponding spectroscopic (*Z*′′(f)) plots of Ag100*x*, *x*=0, 0.02 and 0.04, ceramics measured in the temperature range of 425−550°C

Commonly, the single semicircle indicates that there is a single relaxation time in the sample. However, double relaxations can also appear as single semicircle in the *Z** plot if the resistance of one electroactive region is much higher (e.g., two orders of magnitude or higher) than the other [57]. Thus, to resolve this ambiguity and provide more detailed analysis, the IS data were replotted by using a combination of impedance *Z′′(f)* and electric modulus *M′′(f)* spectroscopic plots, as shown for a sample temperature at 500°C for BNBT, Ag2 and Ag4 compositions in Fig. 7(a)−(c). Furthermore, the resistance (*R*) and dielectric permittivity (ε_r) values associated with each electroactive region in the sample (e.g., grain, grain boundary) can be calculated by the maximum value of $Z''(Z''_{max})$ and $M''(M''_{max})$ according to equations (1) and (2):

$$Z''_{max} = \frac{R}{2} \quad (1)$$

$$M''_{max} = \frac{C_0}{2C} = \frac{1}{2\varepsilon_r} \quad (2)$$

Where *R, C* are the resistance and capacitance values of the resistor and capacitor that represent each electroactive region [52]. The resistivity (ρ) is subsequently obtained through the relation $\rho=RA/L$, where *A* and *L* are sample's area and thickness, respectively. The ρ and ε_r values extracted from the bulk component (at 450°C, 500°C and 550°C) are listed in Table 3.

According to Fig. 7(a), the BNBT composition obviously showed a single Debye-like peak in both *Z′′(f)* and *M′′(f)* plots with frequencies of the *Z′′* and *M′′* peaks that were almost coincident. The full width at half maximum (FWHM), calculated from the normalized *Z′′*(f) spectra, was 1.30 decades (the theoretical value for ideal Debye-like peak=1.14 decades [58]). A single Debye-like peak was still observed in Ag2. However, the peak shape broadened

(FWHM = 1.50 decades) and the frequencies of Z'' and M'' peaks slightly shifted further apart. Finally, when Ag doping content increased to 0.04, two Debye-like peaks were clearly observed in the M'' spectra of Ag4 (see Fig. 7(c)). Typically, the magnitude of Z'' maxima is controlled by the region with largest resistance (R) associated with the grain boundary while that of M'' maxima is dominated by the region with smaller capacitance (C) involving the bulk [59]. Thus, the observed dominant Z'' peak (matching the minor M'' peak in the $M''(f)$ spectra) at lower frequency indicates the grain boundary response, whereas the dominant M'' peak at higher frequency suggests the grain (bulk) response. The evolution of the Debye-like peak in the $Z''(f)$ and $M''(f)$ plot, from a single and slim peak (for BNBT) that becomes broadened (for Ag2) and finally separates into two peaks (for Ag4), clearly supports the observed Z^* data and confirms that acceptor doping Ag into 0.93BNT-0.07BT can cause a change from a homogeneous to a heterogeneous electrical microstructure.

Furthermore, the ε_r values calculated from the main peak in the M'' spectra by using Eq. (2) (see Table II) were comparable to those obtained by the direct temperature dependence dielectric (ε_r-T) measurements in Fig. (3) [e.g., ε_r~3370 (from calculation) and ε_r~2780 (from direct measurement), for Ag2 at 450°C]. This indicates that the dominant M'' peak at higher frequency truly belongs to bulk (grain) response. Beside this, it can be clearly seen from Table 3 that the resistivity considerably decreased (~1 order of magnitude) from 7.2×10^6 Ω.cm (BNBT) to 3.1×10^5, for Ag2, and then only showed a small reduction to 1.5×10^5 Ω.cm (Ag4). The observed result is well consistent with a previous study of Fe acceptor doped BNT and BNT-6BT where a substantial decrease in resistivity (by approximately one order of magnitude) was reported at 2 mol% doping content, beyond this level, only a small change was observed [46].

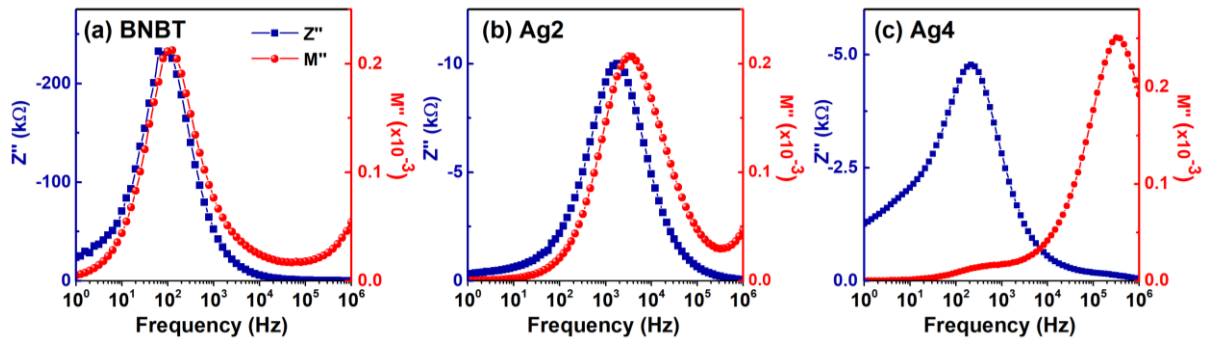

Fig. 7. The $Z'(f)$ and $M'(f)$ spectroscopic plots at 500°C of Ag100x ceramics for (a) x=0, (b) x=00.02 and (c) x=0.04.

Table 3 Bulk resistivity (ρ) and permittivity (ε_r) values extracted from the $Z''(f)$ plots and the activation energy of conduction (E_a) obtained through the Arrhenius plot of BNBT, Ag2 and Ag4 compositions.

Compositions	450°C		500°C		550°C		E_a
	ρ (Ω cm)	ε_r	ρ (Ω cm)	ε_r	ρ (Ω cm)	ε_r	(eV)
BNBT	3.8×10^7	3270	7.2×10^6	2350	2.0×10^6	1740	1.50
Ag2	6.5×10^5	3370	3.1×10^5	2420	1.5×10^5	1840	0.72
Ag4	4.6×10^5	2790	1.5×10^5	1990	5.3×10^4	1550	1.05

To obtain the activation energy of conduction (E_a), the Arrhenius plots of natural log of bulk conductivity ($\ln\sigma$) versus inverse of temperature (1000/T) were utilized as shown in Fig. 8 for BNBT, Ag2 and Ag4 compositions. The solid lines represent the best least-square fitting of the experimental data to the Arrhenius equation:

$$\sigma = \sigma_0 \exp(-\frac{E_a}{k_B T}) \qquad (3)$$

where σ and σ_0 are the dc conductivity and the pre-exponential constant, respectively, k_B is the Boltzmann constant, and T is the absolute temperature. The E_a values of the studied compositions are summarized in Table II. For BNBT, the resultant E_a of 1.50 eV agrees well with the value obtained from similar studies of BNT-BT materials [45] [60]. Additionally, the E_a value of BNBT is also close to half of the band gap values for BNT-BT systems (E_g ~ 3.25−3.4 eV [61][62]), which suggests that the conduction mechanism in BNBT is dominated by intrinsic band-type conduction. With increasing Ag doping content, the magnitude of E_a

significantly dropped to 0.72 eV (for Ag2) and 1.05 eV (for Ag4). A decrease in E_a is known to originate from the existence of additional energy level within the bandgap introduced by the defects. In this study, the most likely defects responsible for electrical conduction at temperature range being investigated are the oxygen vacancies, which are formed by acceptor doping of Ag^+ onto the A-site according to the following defect equation:

$$2TiO_2 + Ag_2O \xrightarrow{2ATiO_3} 2Ag'_A + V_O^{\bullet\bullet} + 2Ti_{Ti}^X + 5O_O^X \qquad (4)$$

where A = $Bi_{0.465}Na_{0.465}Ba_{0.07}$.

The decrease in E_a to 0.72 eV (Ag2) and 1.05 eV (Ag4) is also in accordance with the E_a values (1.005−1.094 eV) reported for the migration of doubly ionized oxygen vacancies ($V_o^{\bullet\bullet}$) at high temperature [63] [64] [65].

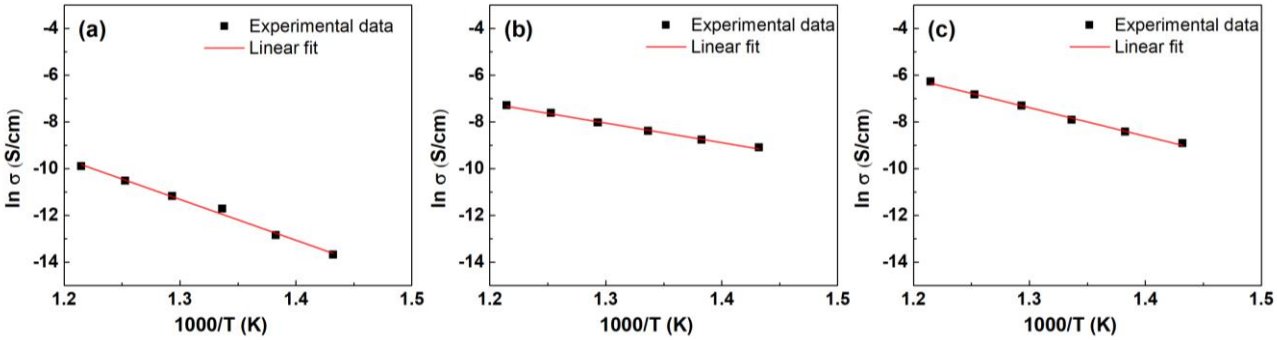

Fig. 8 Arrhenius-type plot of bulk conductivity for Ag100*x* (a) BNBT (b) Ag2 and (c) Ag4.

Figure 9(a) demonstrates room temperature standard *P-E* hysteresis loops of BNBT-*x*Ag, *x*=0.01−0.04, ceramics measured at 60 kV/cm and frequency of 1 Hz. The extracted values of P_r, E_c and P_m are listed in Table 4. A typical square ferroelectric (i.e., non-ergodic relaxor) *P-E* hysteresis loop were observed for BNBT with relatively high values of E_c, P_r and P_m, that are well consistent with earlier studies of the same composition [66] [67]. With increasing *x* to 0.01, the Ag1 composition exhibited pinched *P-E* loop with a substantial drop in E_c (from 28.8 kV/cm to 17.2 kV/cm, ~40%,) while only a slight change in P_r (~7%, from

28.5 to 26.5 μC/cm^2) and P_m (~2%, from 34.7 to 35.4 μC/cm^2) was observed. As x increased to 0.02 (Ag2), the square *P-E* loop was noticed again with an increase in E_c, P_r and P_m. It is worth noting that even though the magnitude of E_c for Ag2 was significantly higher than that of Ag1, it was still lower than the E_c value obtained from the unmodified BNBT. Interestingly, the values of P_r and P_m for Ag2 are the highest. With further increase in x to 0.03 and 0.04, broadened square *P-E* loop was observed. The E_c continuously increased to the maximum value of 34.8 kV/cm (Ag4), while the P_r and P_m progressively dropped to the minimum value of 18.5 and 20.7 μC/cm^2, respectively. Such an increase in E_c and a decrease in P_r and P_m evidently indicate hardening characteristics commonly observed in conventional acceptor doped PZT or BT ferroelectrics due to the stabilized domain configuration [7] [5].

In addition to the true ferroelectric (i.e., remanent or intrinsic) contribution, the standard *P-E* hysteresis loop also includes non-remanent responses (e.g., diode effects, linear resistance, and, in particular, the contribution from leakage current or conductivity) [68] [69]. This can markedly alter the *P-E* loop feature and subsequently lead to the misinterpretation the *P-E* hysteresis loop data. To clarify this issue, the remanent *P-E* hysteresis measurements were carried out on all Ag100x, x=0−0.04, samples as shown in Fig. 9(b). Table 4 demonstrated the extracted values of E_c, P_r and P_m from remanent *P-E* hysteresis loops. In all samples, excellent agreement between remanent and standard *P-E* hysteresis loop data was clearly observed. These include pinched *P-E* loop with significant drop in E_c (for Ag1), the resuming of square *P-E* loop with the highest P_r and P_m values (for Ag2). And finally, the rectangular-shaped *P-E* loop with a substantial increase in E_c along with a reduction in P_r and P_m (for Ag3 and Ag4), which is an indication of hardening characteristics. Since the remanent *P-E* hysteresis loop data are free from the artifacts from conduction, the observed changes in *P-E* loop genuinely arise from ferroelectric contribution within the sample.

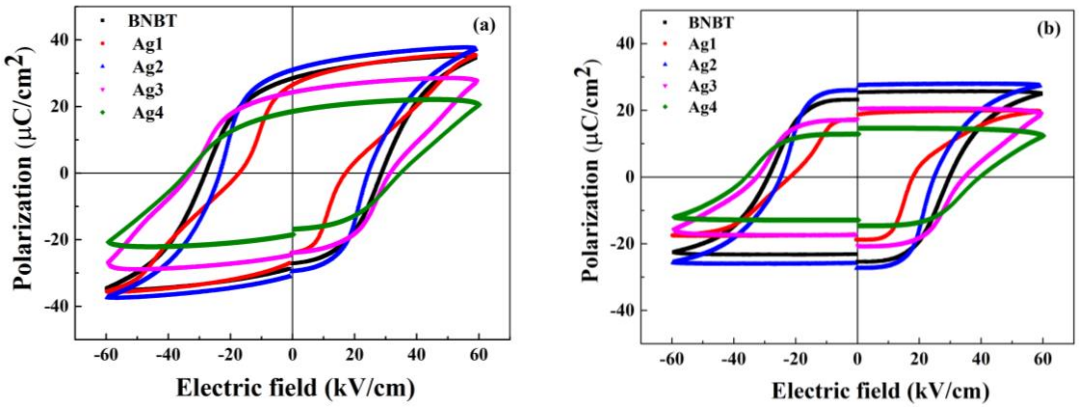

Fig. 9 (a) standard *P-E* hysteresis loops and (b) remanent *P-E* hysteresis loops of BNBT-*x*Ag, *x*=0.01−0.04 ceramics measured under applied electric field of 60 kV/cm at 1 Hz.

Table 4 Values of E_c, P_r and P_m extracted from standard and remanent *P-E* loops of Ag100*x*, *x*=0.0−0.04, samples.

Compositions	Standard *P-E* loops			Remanent *P-E* loops			d_{33} (pC/N)
	E_c (kV/cm)	P_r (μC/cm²)	P_m (μC/cm²)	E_c (kV/cm)	P_r (μC/cm²)	P_m (μC/cm²)	
BNBT	28.8	28.5	34.7	29.8	25.4	24.9	159.2
0.01	17.2	26.5	35.4	17.9	18.8	19.7	145.4
0.02	24.3	30.9	37.4	24.7	27.4	27.4	164.2
0.03	31.6	24.4	27.5	34.8	20.7	18.8	138.0
0.04	34.8	18.5	20.7	39.5	14.6	12.5	127.4

According to the abovementioned results (dielectric, ferroelectric and piezoelectric properties), the observed data can be separated into two regimes: 1) at low level doping (*x*=0.01−0.02), which exhibited the characteristics of domain destabilization and 2) at higher of *x*=0.03−0.04, where the hardening characteristics were observed. For the first regime, a clear transition from a square (BNBT) to a constricted *P-E* loop (Ag1) with large drop in E_c (%40) and a minor change in P_m and P_r was observed. Supporting the *P-E* data, dielectric properties results demonstrated a substantial decrease in T_{F-R} (from 87 to 54°C) along with an increase in tanδ, ε_r and d_{33}, which are all the indication that domain wall movement becomes easier. Normally, by acceptor doping, hardening characteristics like an increase in E_c along with a decrease in P_r, tanδ, ε_r and d_{33} would be expected due to the stabilization of domain configuration or impeding of the domain wall movement by defects or defect dipoles in the

sample [7]. Thus, the observed results in Ag1 composition suggested that there is a competing mechanism to the stabilization of domain. In this study, the plausible explanation would be the "randomizing effect" caused by the addition of Ag^{+}. The A-site in the unit cell of BNT-BT is originally shared by Bi^{3+} Na^{+} and Ba^{+} ions with different size and valence state. The addition of Ag^{+} could increase the degree of disordering on the A-site, leading to the reduction of correlation length between the dipoles, which subsequently disrupt the long-range ferroelectric order [70]. Compared to Ag1, the value of E_c (for Ag2) substantially increased but it is still lower than that of the unmodified BNBT. Meanwhile, an increase in $T_{F\text{-}R}$ (which again is still lower than the observed value for BNBT) along with a decrease in tanδ and ε_r were observed. Moreover, a significant increase in resistivity (~1 order of magnitude) in Ag2 help confirm a considerable increase in defect concentration responsible for the stabilization of domain configuration. The combination of these results suggests an increase in a degree of domain stabilization for Ag2, which still cannot surpass the randomizing effect caused by increasing A-site doping level. It is also worth mentioning that the P_r and P_m values are maximum in Ag2, which correspond well to the highest d_{33}value of 164.2 pC/N.

For the second regime (x=0.03−0.04), a significant increase in E_c and a reduction in P_r and P_m, which are the hardening characteristics commonly observed in PZT, were obviously detected. These data are further supported by a decrease in tanδ, ε_r, and d_{33}, which again indicate that the material became more hardened. Generally, the *P-E* loop characteristics are also affected by the amount of phase constituents [69]. It has been reported in the literature that BNT-based materials with a coexistence of *R3c* and *P4bm* phases would have a lower magnitude of E_c for the composition with dominant *P4bm* phase fraction [39] [45]. Therefore, given that the Ag4 has highest amount of *P4bm* phase fraction, the effect of crystal structure on an increase in E_c could be ruled out. Thus, the combined results for Ag3 and Ag4 compositions revealed true hardening characteristics from microscopic origin linked to the

stabilization of domain configuration as was also supported by a dramatic increase in $T_{F\text{-}R}$ from 87 (BNBT) to 105°C (Ag4).

Conclusion

In summary, dense and single-phase perovskite Ag^+ doped 0.93BNT-0.07BT (Ag100x, x=0.01−0.04) ceramics were successfully obtained by conventional solid-state mixed oxide route. With increasing x, the *P4bm/R3c* phase ratio increased from 25.6%/74.4% (BNBT) to 69.3%/30.7% (Ag4). Increasing Ag^+ dopant led to a decrease in resistivity (~1 order of magnitude), a transition to heterogeneous electrical microstructure consisting of bulk and grain boundary, and a decrease in E_a from 1.50 eV to 1.05 eV. The electromechanical properties revealed amphoteric effects based on the amount of dopant. At low level doping (x=0.01−0.02), the softening-like characteristics: a decrease in E_c and increases in P_r, P_m, ε_r, $\tan\delta$, and d_{33}, were observed. On the contrary, higher doping level (x=0.03−0.04) revealed a substantial increase in E_c and decreases in P_r, P_m, ε_r, $\tan\delta$, and d_{33}, which are all typical characteristics of hardening effects in PZT. The observed results suggest a dominant of randomizing effect at the low level of doping, as was supported by a decrease in $T_{F\text{-}R}$ from 87°C (BNBT) to 54°C and 66°C (Ag2). Meanwhile, the observed hardening effects at higher doping level indicate the more stabilization domain configurations from the defects, as evidenced by ~1 order of magnitude increase in conductivity and a substantial increase in $T_{F\text{-}R}$ (~20°C, from 87 for BNBT to 105°C for Ag4). The results from this study contribute a more understanding on the effects of A-site acceptor doping on the properties of BNT-BT, which will be useful for the designing of this family of materials for the practical applications.

Acknowledgement

This work is financially supported by the Air Force Office of Scientific Research under award number FA2386-21-1-4130.

References

[1] B. Jaffe, W.R. Cook, H. Jaffe, Piezoelectric Ceramics, Academic Press, New York, 1971.

[2] K. Uchino, J. Zheng, Y. Chen, X. Du, J. Ryu, Y. Gao, S. Ural, S. Priya, S. Hirose, Loss mechanisms and high power piezoelectrics, J. Mater. Sci. 41 (2006) 217–228.

[3] K. Uchino, Piezoelectric ultrasonic motors: overview, Smart Mater. Struct. 7 (1998) 273.

[4] W. Jo, R. Dittmer, M. Acosta, J. Zang, C. Groh, E. Sapper, K. Wang, J. Rödel, Giant electric-field-induced strains in lead-free ceramics for actuator applications–status and perspective, J. Electroceramics. 29 (2012) 71–93.

[5] D. Damjanovic, Ferroelectric, dielectric and piezoelectric properties of ferroelectric thin films and ceramics, Rep. Prog. Phys. 61 (1998) 1267.

[6] L.-X. He, M. Gao, C.-E. Li, W.-M. Zhu, H.-X. Yan, Effects of Cr_2O_3 addition on the piezoelectric properties and microstructure of PbZrxTiy (Mg1/3Nb2/3) 1− x− yO3 ceramics, J. Eur. Ceram. Soc. 21 (2001) 703–709.

[7] S. Zhang, J.B. Lim, H.J. Lee, T.R. Shrout, Characterization of hard piezoelectric lead-free ceramics, IEEE Trans. Ultrason. Ferroelectr. Freq. Control. 56 (2009) 1523–1527.

[8] D. Mahato, R. Chaudhary, S. Srivastava, Effect of Na on microstructure, dielectric and piezoelectric properties of PZT ceramic, J. Mater. Sci. Lett. 22 (2003) 1613–1615.

[9] K. Carl, K. Hardtl, Electrical after-effects in $Pb(Ti, Zr)O_3$ ceramics, Ferroelectrics. 17 (1977) 473–486.

[10] J. Glaum, Y.A. Genenko, H. Kungl, L. Ana Schmitt, T. Granzow, De-aging of Fe-doped lead-zirconate-titanate ceramics by electric field cycling: 180-vs. non-180 domain wall processes, J. Appl. Phys. 112 (2012) 034103.

[11] R.-A. Eichel, Structural and dynamic properties of oxygen vacancies in perovskite oxides—analysis of defect chemistry by modern multi-frequency and pulsed EPR techniques, Phys. Chem. Chem. Phys. 13 (2011) 368–384.

[12] K.J. Puttlitz, G.T. Galyon, Impact of the ROHS Directive on high-performance electronic systems: Part II: key reliability issues preventing the implementation of lead-free solders, J. Mater. Sci. Mater. Electron. 18 (2007) 347–365.

[13] J.M. Schoenung, O.A. Ogunseitan, J.D.M. Saphores, A.A. Shapiro, Adopting lead-free electronics: policy differences and knowledge gaps, J. Ind. Ecol. 8 (2004) 59–85.

[14] Y. Fukuda, S. Fanesan, M. Pecht, Lead-free Legislations, Exemptions, and Compliance, Lead-free Electron. (2006) 45–79.

[15] T. Takenaka, K.M.K. Maruyama, K.S.K. Sakata, $(Bi_{1/2}Na_{1/2})TiO_3$-$BaTiO_3$ system for lead-free piezoelectric ceramics, Jpn. J. Appl. Phys. 30 (1991) 2236.

[16] C. Ma, X. Tan, E. Dul'Kin, M. Roth, Domain structure-dielectric property relationship in lead-free $(1- x)(Bi_{1/2}Na_{1/2})TiO_3$-$xBaTiO_3$ ceramics, J. Appl. Phys. 108 (2010) 104105.

[17] H. Du, Z. Li, F. Tang, S. Qu, Z. Pei, W. Zhou, Preparation and piezoelectric properties of $(K_{0.5}Na_{0.5})NbO_3$ lead-free piezoelectric ceramics with pressure-less sintering, Mater. Sci. Eng. B. 131 (2006) 83–87.

[18] W. Jo, E. Erdem, R.-A. Eichel, J. Glaum, T. Granzow, D. Damjanovic, J. Rödel, Effect of Nb-donor and Fe-acceptor dopants in (Bi 1/2 Na 1/2) TiO 3–BaTiO 3–(K 0.5 Na 0.5) NbO 3 lead-free piezoceramics, J. Appl. Phys. 108 (2010) 014110.

[19] E. Aksel, E. Erdem, P. Jakes, J.L. Jones, R.-A. Eichel, Defect structure and materials "hardening" in Fe_2O_3-doped $[Bi_{0.5}Na_{0.5}]TiO_3$ ferroelectrics, Appl. Phys. Lett. 97 (2010) 012903.

[20] C. Lee, H. Han, T.A. Duong, T.H. Dinh, C.W. Ahn, J. Lee, Stabilization of the relaxor phase by adding CuO in lead-free $(Bi_{1/2}Na_{1/2})TiO_3$–$SrTiO_3$–$BiFeO_3$ ceramics, Ceram. Int. 43 (2017) 11071–11077.

[21] M. Li, M.J. Pietrowski, R.A. De Souza, H. Zhang, I.M. Reaney, S.N. Cook, J.A. Kilner, D.C. Sinclair, A family of oxide ion conductors based on the ferroelectric perovskite $Na_{0.5}Bi_{0.5}TiO_3$, Nat. Mater. 13 (2014) 31–35.

[22] Y. Hiruma, H. Nagata, T. Takenaka, Thermal depoling process and piezoelectric properties of bismuth sodium titanate ceramics, J. Appl. Phys. 105 (2009) 084112.

[23] X. Liu, H. Fan, J. Shi, L. Wang, H. Du, Enhanced ionic conductivity of Ag addition in acceptor-doped $Bi_{0.5}Na_{0.5}TiO_3$ ferroelectrics, RSC Adv. 6 (2016) 30623–30627.
[24] D.P. Shih, A. Aguadero, S.J. Skinner, Improvement of ionic conductivity in A-site lithium doped sodium bismuth titanate, Solid State Ion. 317 (2018) 32–38.
[25] T.H. Dinh, M.R. Bafandeh, J.-K. Kang, C.-H. Hong, W. Jo, J.-S. Lee, Comparison of structural, ferroelectric, and strain properties between A-site donor and acceptor doped $Bi_{1/2}(Na_{0.82}K_{0.18})_{1/2}TiO_3$ ceramics, Ceram. Int. 41 (2015) S458–S463.
[26] S. Prasertpalichat, S. Khengkhatkan, T. Siritanon, J. Jutimoosik, P. Kidkhunthod, T. Bongkarn, E.A. Patterson, Comparison of structural, ferroelectric, and piezoelectric properties between A-site and B-site acceptor doped $0.93Bi_{0.5}Na_{0.5}TiO_3$-$0.07BaTiO_3$ lead-free piezoceramics, J. Eur. Ceram. Soc. 41 (2021) 4116–4128.
[27] R. Ranjan, A. Dviwedi, Structure and dielectric properties of $(Na_{0.50}Bi_{0.50})_{1-x}Ba_xTiO_3$: $0 \leq x \leq 0.10$, Solid State Commun. 135 (2005) 394–399.
[28] J.E. Daniels, W. Jo, J. Rödel, V. Honkimäki, J.L. Jones, Electric-field-induced phase-change behavior in $(Bi_{0.5}Na_{0.5})TiO_3$–$BaTiO_3$–$(K_{0.5}Na_{0.5})NbO_3$: A combinatorial investigation, Acta Mater. 58 (2010) 2103–2111.
[29] J.E. Daniels, W. Jo, J. Rödel, J.L. Jones, Electric-field-induced phase transformation at a lead-free morphotropic phase boundary: Case study in a $93\%(Bi_{0.5}Na_{0.5})TiO_3$–$7\%BaTiO_3$ piezoelectric ceramic, Appl. Phys. Lett. 95 (2009) 032904.
[30] J. Kling, X. Tan, W. Jo, H. Kleebe, H. Fuess, J. Rödel, In situ transmission electron microscopy of electric field-triggered reversible domain formation in Bi-based lead-free piezoceramics, J. Am. Ceram. Soc. 93 (2010) 2452–2455.
[31] L.A. Schmitt, H.-J. Kleebe, Single grains hosting two space groups—a transmission electron microscopy study of a lead-free ferroelectric, Funct. Mater. Lett. 3 (2010) 55–58.
[32] R.T. Shannon, C.T. Prewitt, Effective ionic radii in oxides and fluorides, Acta Crystallogr. B. 25 (1969) 925–946.
[33] R.D. Shannon, Revised effective ionic radii and systematic studies of interatomic distances in halides and chalcogenides, Acta Crystallogr. A. 32 (1976) 751–767.
[34] W. Ge, C. Luo, Q. Zhang, Y. Ren, J. Li, H. Luo, D. Viehland, Evolution of structure in $Na_{0.5}Bi_{0.5}TiO_3$ single crystals with BaTiO3, Appl. Phys. Lett. 105 (2014) 162913.
[35] R. Garg, B. Narayana Rao, A. Senyshyn, R. Ranjan, Long ranged structural modulation in the pre-morphotropic phase boundary cubic-like state of the lead-free piezoelectric $Na_{1/2}Bi_{1/2}TiO_3$-$BaTiO_3$, J. Appl. Phys. 114 (2013) 234102.
[36] J. Zhao, N. Zhang, W. Ren, G. Niu, D. Walker, P.A. Thomas, L. Wang, Z. Ye, Polar domain structural evolution under electric field and temperature in the $(Bi_{0.5}Na_{0.5})TiO_3$-$0.06BaTiO_3$ piezoceramics, J. Am. Ceram. Soc. 102 (2019) 437–447.
[37] D. Maurya, M. Murayama, A. Pramanick, W.T. Reynolds Jr, K. An, S. Priya, Origin of high piezoelectric response in A-site disordered morphotropic phase boundary composition of lead-free piezoelectric $0.93(Na_{0.5}Bi_{0.5})TiO_3$–$0.07\ BaTiO_3$, J. Appl. Phys. 113 (2013) 114101.
[38] S. Prasertpalichat, T. Siritanon, N. Nuntawong, D.P. Cann, Structural characterization of A-site nonstoichiometric $(1-x)Bi_{0.5}Na_{0.5}TiO_3$–$xBaTiO_3$ ceramics, J. Mater. Sci. 54 (2019) 1162–1170.
[39] G. Viola, R. McKinnon, V. Koval, A. Adomkevicius, S. Dunn, H. Yan, Lithium-induced phase transitions in lead-free $Bi_{0.5}Na_{0.5}TiO_3$ based ceramics, J. Phys. Chem. C. 118 (2014) 8564–8570.
[40] X. Liu, J. Shi, F. Zhu, H. Du, T. Li, X. Liu, H. Lu, Ultrahigh energy density and improved discharged efficiency in bismuth sodium titanate based relaxor ferroelectrics with A-site vacancy, J. Materiomics. 4 (2018) 202–207.
[41] B. Parija, T. Badapanda, P.K. Sahoo, M. Kar, P. Kumar, S. Panigrahi, Structural and electromechanical study of $Bi_{0.5}Na_{0.5}TiO_3$-$BaTiO_3$ solid-solutions, Process. Appl. Ceram. 7 (2013) 73–80.
[42] L.A. Schmitt, J. Kling, M. Hinterstein, M. Hoelzel, W. Jo, H.-J. Kleebe, H. Fuess, Structural investigations on lead-free $Bi_{1/2}Na_{1/2}TiO_3$-based piezoceramics, J. Mater. Sci. 46 (2011) 4368–4376.
[43] L.A. Schmitt, M. Hinterstein, H.-J. Kleebe, H. Fuess, Comparative study of two lead-free piezoceramics using diffraction techniques, J. Appl. Crystallogr. 43 (2010) 805–810.

[44] W. Jo, S. Schaab, E. Sapper, L.A. Schmitt, H.-J. Kleebe, A.J. Bell, J. Rödel, On the phase identity and its thermal evolution of lead free $(Bi_{1/2}Na_{1/2})TiO_3$-6 mol% $BaTiO_3$, J. Appl. Phys. 110 (2011) 074106.
[45] Q. Xu, H. Liu, L. Zhang, J. Xie, H. Hao, M. Cao, Z. Yao, M.T. Lanagan, Structure and electrical properties of lead-free $Bi_{0.5}Na_{0.5}TiO_3$-based ceramics for energy-storage applications, Rsc Adv. 6 (2016) 59280–59291.
[46] S. Steiner, I. Seo, P. Ren, M. Li, D.J. Keeble, T. Frömling, The effect of Fe-acceptor doping on the electrical properties of $Na_{1/2}Bi_{1/2}TiO_3$ and $0.94(Na_{1/2}Bi_{1/2})TiO_3$–$0.06BaTiO_3$, J. Am. Ceram. Soc. 102 (2019) 5295–5304.
[47] S. Schaab, T. Granzow, Temperature dependent switching mechanism of $(Pb_{0.92}La_{0.08})(Zr_{0.65}Ti_{0.35})O_3$ investigated by small and large signal measurements, Appl. Phys. Lett. 97 (2010) 132902.
[48] H. Zhang, J. Zhou, W. Chen, X. Yang, J. Shen, C. Wu, Stabilization of Ferroelectric Order in $Bi_{1/2}(Na_{0.8}K_{0.2})_{1/2}TiO_3$ Lead-Free Ceramics with Fe Doping, J. Electron. Mater. 46 (2017) 6167–6174.
[49] J. Han, J. Yin, J. Wu, $(Bi_{0.5}Na_{0.5})TiO_3$ ferroelectric ceramics: Achieving high depolarization temperature and improved piezoelectric properties, J. Eur. Ceram. Soc. 40 (2020) 5392–5401.
[50] J. Xu, Q. Li, L. Yang, W. Zeng, C. Zhou, C. Yuan, G. Chen, G. Rao, Effects of thermal and electrical histories on structure and dielectric behaviors of $(Li_{0.5}Nd_{0.5})^{2+}$-modified $(Bi_{0.5}Na_{0.5})TiO_3$-$BaTiO_3$ ceramics, J. Materiomics. 3 (2017) 121–129.
[51] L. Wang, C. Zhu, L. Chen, C. Li, S. Yuan, Room-temperature magnetoelectric coupling study of multiferroic $(1- x)(0.7BiFeO_3$-$0.3Bi_{0.5}Na_{0.5}TiO_3)$-$xCoFe_2O_4$ ceramics, J. Sol-Gel Sci. Technol. 82 (2017) 184–192.
[52] J. Zang, M. Li, D.C. Sinclair, W. Jo, J. Rödel, Impedance spectroscopy of $(Bi_{1/2}Na_{1/2})TiO_3$–$BaTiO_3$ ceramics modified with (K 0.5 Na 0.5) NbO 3, J. Am. Ceram. Soc. 97 (2014) 1523–1529.
[53] S. Sahoo, S. Hajra, M. De, R. Choudhary, Resistive, capacitive and conducting properties of $Bi_{0.5}Na_{0.5}TiO_3$-$BaTiO_3$ solid solution, Ceram. Int. 44 (2018) 4719–4726.
[54] Y. Huang, D. Shi, L. Liu, G. Li, S. Zheng, L. Fang, High-temperature impedance spectroscopy of $BaFe_{0.5}Nb_{0.5}O_3$ ceramics doped with $Bi_{0.5}Na_{0.5}TiO_3$, Appl. Phys. A. 114 (2014) 891–896.
[55] Q. Xu, M.T. Lanagan, W. Luo, L. Zhang, J. Xie, H. Hao, M. Cao, Z. Yao, H. Liu, Electrical properties and relaxation behavior of $Bi_{0.5}Na_{0.5}TiO_3$-$BaTiO_3$ ceramics modified with NaNbO3, J. Eur. Ceram. Soc. 36 (2016) 2469–2477.
[56] B. Barick, R. Choudhary, D. Pradhan, Dielectric and impedance spectroscopy of zirconium modified $(Na_{0.5}Bi_{0.5})TiO_3$ ceramics, Ceram. Int. 39 (2013) 5695–5704.
[57] D.C. Sinclair, A.R. West, Impedance and modulus spectroscopy of semiconducting $BaTiO_3$ showing positive temperature coefficient of resistance, J. Appl. Phys. 66 (1989) 3850–3856.
[58] D. Sinclair, A. West, Effect of atmosphere on the PTCR properties of $BaTiO_3$ ceramics, J. Mater. Sci. 29 (1994) 6061–6068.
[59] F.D. Morrison, D.C. Sinclair, A.R. West, Characterization of lanthanum-doped barium titanate ceramics using impedance spectroscopy, J. Am. Ceram. Soc. 84 (2001) 531–538.
[60] S. Prasertpalichat, W. Schmidt, D.P. Cann, Effects of A-site nonstoichiometry on oxide ion conduction in $0.94Bi_{0.5}Na_{0.5}TiO_3$–$0.06BaTiO_3$ ceramics, J. Adv. Dielectr. 6 (2016) 1650012.
[61] M. Cernea, L. Trupina, C. Dragoi, A.-C. Galca, L. Trinca, Structural, optical, and electric properties of BNT–$BT_{0.08}$ thin films processed by sol–gel technique, J. Mater. Sci. 47 (2012) 6966–6971.
[62] M. Cernea, A.C. Galca, M.C. Cioangher, C. Dragoi, G. Ioncea, Piezoelectric BNT-$BT_{0.11}$ thin films processed by sol–gel technique, J. Mater. Sci. 46 (2011) 5621–5627.
[63] R. Waser, T. Baiatu, K. Härdtl, dc electrical degradation of perovskite-type titanates: I, Ceramics, J. Am. Ceram. Soc. 73 (1990) 1645–1653.
[64] R. Waser, T. Baiatu, K. Härdtl, Dc electrical degradation of perovskite-type titanates: II, single crystals, J. Am. Ceram. Soc. 73 (1990) 1654–1662.
[65] T. Baiatu, R. Waser, K. Härdtl, Dc electrical degradation of perovskite-type titanates: III, a model of the mechanism, J. Am. Ceram. Soc. 73 (1990) 1663–1673.

[66] S. Prasertpalichat, D.P. Cann, Hardening in non-stoichiometric $(1- x)Bi_{0.5}Na_{0.5}TiO_3–xBaTiO_3$ lead-free piezoelectric ceramics, J. Mater. Sci. 51 (2016) 476–486.
[67] L.M. Denis, J. Glaum, M. Hoffman, J.E. Daniels, R.J. Hooper, G. Tutuncu, J.S. Forrester, J.L. Jones, Effect of mechanical depoling on piezoelectric properties of $Na_{0.5}Bi_{0.5}TiO_3–xBaTiO_3$ in the morphotropic phase boundary region, J. Mater. Sci. 53 (2018) 1672–1679.
[68] M. Dawber, K. Rabe, J. Scott, Physics of thin-film ferroelectric oxides, Rev. Mod. Phys. 77 (2005) 1083.
[69] L. Jin, F. Li, S. Zhang, Decoding the fingerprint of ferroelectric loops: comprehension of the material properties and structures, J. Am. Ceram. Soc. 97 (2014) 1–27.
[70] R. Dittmer, W. Jo, J. Daniels, S. Schaab, J. Rödel, Relaxor characteristics of morphotropic phase boundary $(Bi_{1/2}Na_{1/2})TiO_3–(Bi_{1/2}K_{1/2})TiO_3$ modified with $Bi(Zn_{1/2}Ti_{1/2})O_3$, J. Am. Ceram. Soc. 94 (2011) 4283–4290.

Accomplishments

1. The data from this study were written into a manuscript and are in the process of being submitted to a high-impact factor journal.
2. Part of the data from this study was included in the presentation to present in an international conference.

   Presentation title: “Comparative study between the effects of A-site and B-site acceptor doping on the hardening characteristics of BNTBT lead-free piezoceramics”

   Type of presentation: Oral presentation (invited speaker)

   Conference detail: “International Conference and Exhibition on Science, Technology, and Engineering of Materials (ISTEM 2022)” held at Nongnooch traditional conference center, Pattaya, Thailand, during 29th November 2022 to 2nd December 2022
3. PI, together with one graduate student, visited Oregon State University as proposed in the proposal from April 14th, 2022 to June 12th, 2022. The purpose of the visit was to characterize the electrical properties of the samples and to explore the possibility of collaboration with the PI’s advisor, Prof. David P. Cann, in the future.

Impacts

1. During the past 20 years, the search for environmentally friendly, lead-free piezoceramics with comparable properties to their lead-based counterparts has been the

main quest in the community. Among the available lead-free piezoelectric ceramics, the (1-*x*)$Bi_{0.5}Na_{0.5}TiO_3$-*x*$BaTiO_3$ solid solution is considered one of the most promising candidates due to its excellent dielectric and piezoelectric properties, as well as its relatively simple preparation. However, the understanding of the "hardening effect" in lead-free piezoceramics in terms of defect chemistry-property relationships is not well-realized, thereby limiting their usage in real-world applications. In this research, we systematically investigate the effects of A-site doping on the crystal structure, electrical conductivity, and electromechanical properties. The findings from this study are expected to provide a better understanding of the effect of hard doping in BNT-based ceramics, which can aid in the more reliable modification of these materials for practical applications.